Electron-Following Mapping Transformations from the Electronegativity Equalization Principle

Roman F. Nalewajski* and Olga Sikora

K. Gumiński Department of Theoretical Chemistry, Jagiellonian University, R. Ingardena 3, 30-060 Cracow, Poland

Received: January 31, 2000; In Final Form: March 29, 2000

The so-called electron-following (EF) mapping relations for the closed molecular systems are derived within the charge sensitivity analysis (CSA) in atomic resolution, using the electronegativity equalization principle of Sanderson. They are tested on selected small molecules and model molecular adducts. For the fixed overall charge Q of a given molecular system, these relations determine the transformation $\mathbf{T}(\mathbf{Q} \rightarrow \mathbf{q})_Q = (\partial \mathbf{q}/\partial \mathbf{Q})_Q$ of displacements $\Delta\mathbf{Q}$ in the nuclear coordinates $\mathbf{Q}$ (perturbations) into the concomitant shifts $(\Delta\mathbf{q})_Q$ of atomic charges $\mathbf{q}$ (responses): $(\Delta\mathbf{q})_Q = \Delta\mathbf{Q}\ \mathbf{T}(\mathbf{Q} \rightarrow \mathbf{q})_Q$. The differential CSA EF "translators" $\mathbf{T}(\mathbf{Q} \rightarrow \mathbf{q})_Q$ have been determined for diatomics (HX, X = F, Cl, Br), water, ethane, and model molecular complexes (HF- - -HF, H_2O- - -HCl, ClH- - -NH_3). The translator charge variation trends are then numerically validated by comparing them with the corresponding plots obtained from the equilibrium CSA charge distributions for several molecular geometries. The CSA EF charge variations are also compared with those resulting from the reference SCF MO [MNDO, ab initio] and Kohn−Sham calculations and several partitioning schemes of a molecular electron density into atomic charges. The charge variations accompanying bond stretches in HX are found to be strongly dependent on both the method and partitioning scheme applied.

1. Introduction

Each *bond-breaking-bond forming* process in chemistry implies changes in both the *electronic structure*, characterized by the ground-state electron density $\rho(\mathbf{r})$ or its discretized *atoms-in-molecules* (AIM) representation in the form of the AIM electron populations, $\mathbf{N} = (N_1, N_2, ..., N_m)$, normalized to the overall number of electrons in the reactive system, $N = \int \rho(\mathbf{r})\, d\mathbf{r}. = \sum_{i=1}^{m} N_i$, and the *geometrical structure*, defined by the position vectors $\{\mathbf{R}_\alpha\}$ of the nuclei, $\mathbf{Q} = (\mathbf{R}_1, \mathbf{R}_2, ..., \mathbf{R}_m)$. These two structural features are mutually coupled on the hypersurface of the electronic ground-state energy:[1−8]

$$E(N,\mathbf{Q}) = \langle \Psi(N,\mathbf{Q})|\hat{H}(N,\mathbf{Q})|\Psi(N,\mathbf{Q})\rangle = E[N,v(\mathbf{Q})] = E_{v(\mathbf{Q})}[\rho(\mathbf{Q})] \quad (1)$$

where $\hat{H}(N, \mathbf{Q})$ is the electronic Hamiltonian, $\Psi(N,\mathbf{Q})$ stands for its ground state, $v(\mathbf{Q})$ is the external potential due to nuclei, and $E_v[\rho]$ denotes the density functional for the energy.[9,10]

The corresponding Euler equation for the equilibrium distribution of electrons, e.g., the Kohn−Sham (KS)[9] equations of the density-functional theory (DFT)[9−12] for the assumed molecular geometry $\mathbf{Q}$ (Born−Oppenheimer approximation), then determines $\rho(\mathbf{r})$ (or $\mathbf{N}$), which parametrically depends on the geometrical structure: $\rho(\mathbf{r}) = \rho(\mathbf{Q};\mathbf{r})$ [or $\mathbf{N} = \mathbf{N}(\mathbf{Q})$]. Therefore, such a procedure can be characterized by the following "electron-following" (EF) mappings:[13]

$$\text{EF:} \qquad (\mathbf{Q} \rightarrow \rho) \quad \text{or} \quad (\mathbf{Q} \rightarrow \mathbf{N}) \quad (2)$$

In many qualitative considerations in chemistry, e.g., in the structural rules of Gutmann,[14] the opposite, "electron-preceding" (EP) perspective[15] is adopted, in which displacements of the electron distribution are considered as preceding (accelerating) the nuclear motions:

$$\text{EP:} \qquad (\rho \rightarrow \mathbf{Q}) \quad \text{or} \quad (\mathbf{N} \rightarrow \mathbf{Q}) \quad (3)$$

This approach is in the spirit of the familiar Hellmann−Feynman theorem, which states that the (quantum-mechanical) electron density

$$\rho(\mathbf{r}) = \langle \Psi(N,\mathbf{Q})|\hat{\rho}(N,\mathbf{r})|\Psi(N,\mathbf{Q})\rangle = (\delta E[N,v]/\delta v(\mathbf{r}))_N \quad (4)$$

where $\hat{\rho}(N,\mathbf{r}) = \sum_{i=1}^{N} \delta(\mathbf{r}_i - \mathbf{r})$, determines uniquely the forces $\mathbf{F}(N,\mathbf{Q}) = -\partial E(N,\mathbf{Q})/\partial \mathbf{Q}$ acting on the system nuclei, given by the classical expressions in terms of ρ, and thus also the equilibrium structure $\mathbf{Q}^0$, for which $\mathbf{F}(N,\mathbf{Q}^0) = \mathbf{0}$.

It has been demonstrated recently,[1−8] using standard chain-rule manipulations on derivatives in the atomic description, that the explicit mapping transformations, EP: $\mathbf{T}(\mathbf{N} \rightarrow \mathbf{Q}) \equiv \partial \mathbf{Q}/\partial \mathbf{N}$, and EF: $\mathbf{T}(\mathbf{Q} \rightarrow \mathbf{N}) \equiv \partial \mathbf{N}/\partial \mathbf{Q}$, called "translators", can be derived within the charge sensitivity analysis (CSA)[1,3−8] and the related electronegativity equalization method (EEM),[2] between shifts $\Delta\mathbf{Q}$ in the molecular geometry and the concomitant displacements in the electronic structure, measured by changes in the AIM populations $\Delta\mathbf{N}$ (or atomic charges $\Delta\mathbf{q}$):

$$\text{EP-CSA/AIM: } \Delta\mathbf{Q} = \Delta\mathbf{N}\ \mathbf{T}(\mathbf{N} \rightarrow \mathbf{Q}); \qquad \text{EF-CSA/AIM: } \Delta\mathbf{N} = \Delta\mathbf{Q}\ \mathbf{T}(\mathbf{Q} \rightarrow \mathbf{N}) \quad (5)$$

Similar mapping relations can also be formulated[5,7] within the compliance (minimum energy) approach.[16] These mapping relations can be formulated for both externally open (fluctuating N) and closed (fixed N) molecular systems. The former correspond to the constraint of the fixed chemical potential of the electron reservoir, to which the molecule is coupled, while the latter implies the fixed charge of the system as a whole.

* Corresponding author.

10.1021/jp000372u CCC: $19.00
Published on Web 05/23/2000

The main goal of the present work is to derive these transformations for the closed molecular system from the Sanderson electronegativity equalization principle (EEP)[1,11] and to test the resulting EF-CSA/AIM translators on simple, externally closed molecular systems including molecules (HX, X = F, Cl, Br, water, ethane), and model molecular adducts (HF- - -HF, H_2O- - -HCl, ClH- - -NH_3). In order to validate the mapping derivatives we shall also examine, how these mapping trends exhibited by the AIM charges

$$\mathbf{q} = (q_1, q_2 ..., q_m) = \mathbf{Z} - \mathbf{N} \tag{6}$$

where $\mathbf{Z} = (Z_1, Z_2, ..., Z_m)$ is the row vector of the nuclear atomic numbers, compare with the exact CSA predictions obtained via the repeated CSA calculations for different molecular geometries.

The CSA results will also be compared with those obtained from other methods of determining the electronic structure [SCF MO (ab initio,[17] MNDO[18]) or DFT (LSDA)[19]] and several schemes for partitioning the molecular electron distribution into the atomic populations/charges [Mulliken[20] (M), Bader[21] (B), Hirshfeld[22] (H), and the fitting of atomic charges to the electrostatic potential (ESP)[23]]. The atomic units are used throughout the paper, unless explicitly stated otherwise.

2. Theoretical Background

Quadratic Energy Function and Its Derivatives. The CSA approach in the atomic resolution uses the quadratic Taylor expansion of the ground-state electronic energy $E_v[\rho]$ in terms of the AIM charge displacements $\Delta\mathbf{q} = \mathbf{q} - \mathbf{q}^0$, relative to the neutral atom charges $\mathbf{q}^0 = \mathbf{0}$ ($\mathbf{Z} = \mathbf{N}^0$), i.e., $\Delta\mathbf{q} = \mathbf{q}$, or equivalently in terms of the corresponding shifts in the AIM electron populations, $\Delta\mathbf{N} = \mathbf{N} - \mathbf{N}^0 = \mathbf{N} - \mathbf{Z}$[1-4]

$$E_v[\rho] \approx E(\mathbf{q},\mathbf{Q}) \equiv E(\mathbf{0},\mathbf{Q}) + \Delta\mathbf{q}\frac{\partial E}{\partial \mathbf{q}} + \frac{1}{2}\Delta\mathbf{q}\left(\frac{\partial^2 E}{\partial \mathbf{q}\ \partial \mathbf{q}}\right)\Delta\mathbf{q}^{\mathrm{T}}$$

$$\equiv E^0 + \Delta\mathbf{q}\ \mathbf{u}(\mathbf{q},\mathbf{Q})^{\mathrm{T}} + \frac{1}{2}\Delta\mathbf{q}\ \mathbf{h}\ \Delta\mathbf{q}^{\mathrm{T}}$$

$$\equiv \bar{E}(\mathbf{N},\mathbf{Q}) \equiv \bar{E}(\mathbf{Z},\mathbf{Q}) + \Delta\mathbf{N}\frac{\partial \bar{E}}{\partial \mathbf{N}} + \frac{1}{2}\Delta\mathbf{N}\left(\frac{\partial^2 \bar{E}}{\partial \mathbf{N}\ \partial \mathbf{N}}\right)\Delta\mathbf{N}^{\mathrm{T}}$$

$$\equiv E^0 + \Delta\mathbf{N}\ \mathbf{m}(\mathbf{N},\mathbf{Q})^{\mathrm{T}} + \frac{1}{2}\Delta\mathbf{N}\ \mathbf{h}\ \Delta\mathbf{N}^{\mathrm{T}} \tag{7}$$

where E^0 denotes the energy of the "promolecule", consisting of the neutral atoms shifted from infinity to the actual positions $\mathbf{Q}$ in a molecule, the row vectors $\mathbf{u} = (\chi_1, \chi_2, ..., \chi_m)$ and $\mathbf{m} = (\mu_1, \mu_2, ..., \mu_m) = -\mathbf{u}$ group the electronegativities and chemical potentials, respectively, of the separated atoms, and $\mathbf{h} = \{\eta^0_{i,j}\}$ denotes the hardness matrix in the atomic resolution.

This choice of the promolecule reference state, representing a higly "unphysical" species consisting of the nonequilibrium AIM electron distributions, marked by the nonequalized chemical potentials $\mathbf{m}$ (or electronegativities $\mathbf{u}$) of the promolecule atoms, is convenient for using the isolated atom data to model interactions in a molecule. Clearly, by subsequently determining the equilibrium AIM charge reorganization $\Delta\mathbf{N}$ (or $\Delta\mathbf{q}$), which equalizes the "electronic" forces $\mathbf{m}$ (or $\mathbf{u}$) in a molecule, one eventually includes also the relevant effects of the charge transfer between the promolecule atoms, correct to the second-order of the Taylor expansion of eq 7. These electronegativity equalization equations will be summarized in the next subsection.

The *quadratic energy* of eq 7 can be conveniently decomposed into the geometry-independent atomic energies, $\{E_i(q_i)\}$, and the geometry-dependent diatomic terms, $\{E_{ij}(q_i,q_j)\}$:

$$E(\mathbf{q},\mathbf{Q}) \equiv \sum_{i=1}^{m} E_i(q_i) + \sum_{i=1}^{m-1}\sum_{j=i+1}^{m} E_{ij}(q_i,q_j)$$

$$E_i(q_i) = E_i(q_i{=}0) + \left.\frac{\partial E_i(q_i)}{\partial q_i}\right|_{q_i=0} q_i + \frac{1}{2}\left.\frac{\partial^2 E_i(q_i)}{\partial q_i^2}\right|_{q_i=0} q_i^2$$

$$\equiv E_i^0 + \chi_i^0 q_i + \frac{1}{2}\eta_{ii}^0 q_i^2 \equiv \bar{E}_i(N_i) \tag{8}$$

$$E_{ij}(q_i,q_j) = \frac{1}{2}\left.\frac{\partial^2 E_{ij}(q_i,q_j)}{\partial q_i\ \partial q_j}\right|_{\mathbf{q}=\mathbf{0}} q_i q_j = \frac{1}{2}[\eta_{ij}^0(\mathbf{Q}) + \eta_{ji}^0(\mathbf{Q})]q_i q_j$$

$$= \eta_{ij}^0(\mathbf{Q}) q_i q_j \tag{9}$$

Above, the atomic electronegativity χ_i^0, negative atomic chemical potential $\mu_i^0 = [\partial\bar{E}_i(N_i)/\partial N_i]_{N_i=Z_i} = -\chi_i^0$, is approximated by the Mulliken[24] (unbiased) finite-difference estimate:

$$\chi_i^0 = -\mu_i^0 = (I_i^0 + A_i^0)/2 \tag{10}$$

while the atomic(diagonal) hardness η_{ii}^0 is similarly approximated by the one-center repulsion energy[1,3] γ_i^0 between two electrons occupying the valence-shell s-orbital of the isolated atom i, $s(\mathbf{r},\mathbf{R}_i)$, determined from the atomic ionization potential I_i^0 and electron affinity A_i^0 via the familiar Pariser[25] formula of the semiempirical ZDO-type SCF MO theories:

$$\eta_{ii}^0 \cong \gamma_i^0 \equiv \int\int s_i^2(\mathbf{r},\mathbf{R}_i)\frac{1}{|\mathbf{r}-\mathbf{r}'|}s_i^2(\mathbf{r}',\mathbf{R}_i)\,\mathrm{d}\mathbf{r}\,\mathrm{d}\mathbf{r}'$$

$$\equiv (s_i s_i|s_i s_i) \approx I_i^0 - A_i^0 \tag{11}$$

The diatomic (off-diagonal) hardness $\eta_{ij}^0(\mathbf{Q})$ in the promolecule is similarly approximated[1,3] by the two-center Coulomb repulsion γ_{ij} between two electrons occupying the valence-shell s-orbitals of atoms i and j, respectively. It can be determined using, e.g., the Ohno[26] interpolation formula:

$$\eta_{ij}^0(R_{ij}) \cong \int\int s_i^2(\mathbf{r},\mathbf{R}_i)\frac{1}{|\mathbf{r}-\mathbf{r}'|}s_j^2(\mathbf{r}',\mathbf{R}_j)\,\mathrm{d}\mathbf{r}\,\mathrm{d}\mathbf{r}' \equiv (s_i s_i|s_j s_j) \approx \gamma_{ij}(R_{ij})$$

$$\gamma_{ij}(R_{ij}) = (a_{ij}^2 + R_{ij}^2)^{-1/2}; \quad a_{ij} = 2/(\eta_{ii}^0 + \eta_{jj}^0); \quad R_{ij} = |\mathbf{R}_j - \mathbf{R}_i| \tag{12}$$

Electronegativity Equalization. The diagonal and off-diagonal hardnesses determine the hardness matrix in the CSA/AIM approximation of eq 7

$$\mathbf{h}(\mathbf{0},\mathbf{Q}) = \{\eta_{ij}^0;\ i,j = 1, 2, ..., m\} = \left(\frac{\partial^2 E(\mathbf{q},\mathbf{Q})}{\partial \mathbf{q}\ \partial \mathbf{q}}\right)_{\mathbf{q}=\mathbf{0}} \equiv \left(\frac{\partial \mathbf{u}(\mathbf{q},\mathbf{Q})}{\partial \mathbf{q}}\right)_{\mathbf{q}=\mathbf{0}}$$

$$= \left(\frac{\partial^2 \bar{E}(\mathbf{N},\mathbf{Q})}{\partial \mathbf{N}\ \partial \mathbf{N}}\right)_{\mathbf{N}=\mathbf{Z}} = \left(\frac{\partial \bar{\mathbf{m}}(\mathbf{N},\mathbf{Q})}{\partial \mathbf{N}}\right)_{\mathbf{N}=\mathbf{Z}} \equiv \mathbf{h} \tag{13}$$

which can be used to determine all linear charge responses.[1-8] For example, the changes in the AIM electronegativities for

the current AIM charges **q**, displaced relative to the reference $\mathbf{q}^0 = \mathbf{0}$

$$\mathbf{u}(\mathbf{q},\mathbf{Q}) \equiv \partial E(\mathbf{q},\mathbf{Q})/\partial \mathbf{q} = [\chi_1(\mathbf{q},\mathbf{Q}), \chi_2(\mathbf{q},\mathbf{Q}), ..., \chi_m(\mathbf{q},\mathbf{Q})] \equiv \mathbf{u} \quad (14)$$

with respect to the neutral atomic values $\mathbf{u}^0 = (\chi_1^0, \chi_2^0, ..., \chi_m^0)$, are given by the **q**-gradient of the energy difference

$$\Delta E(\mathbf{q},\mathbf{Q}) \equiv E(\mathbf{q},\mathbf{Q}) - E(\mathbf{0},\mathbf{Q}) \quad (15)$$

A reference to eq 7 shows that

$$\Delta \mathbf{u}^0(\mathbf{q},\mathbf{Q}) \equiv \Delta \mathbf{u}^0 = \mathbf{u}(\mathbf{q},\mathbf{Q}) - \mathbf{u}^0 = \mathbf{qh} \quad (16)$$

Consider now the differences

$$\Delta \mathbf{u}^*(\mathbf{q},\mathbf{Q}) \equiv \mathbf{u}(\mathbf{q},\mathbf{Q}) - \mathbf{u}(\mathbf{q}^*,\mathbf{Q}) \equiv \Delta \mathbf{u}^* = (\mathbf{q} - \mathbf{q}^*)\,\mathbf{h} \equiv \Delta \mathbf{q}^* \mathbf{h} \quad (17)$$

between electronegativities of eq 14 (for the current charges **q**) and their equilibrium values (for the equilibrium charges $\mathbf{q}^*$)

$$\mathbf{u}(\mathbf{q}^*,\mathbf{Q}) \equiv \mathbf{u}^* = \chi \mathbf{1}, \quad \mathbf{1} = (1, 1, ..., 1) \quad (18)$$

which are equalized at the global electronegativity (negative global chemical potential) level:

$$\chi = \partial E(Q,\mathbf{Q})/\partial Q|_{\mathbf{q}=\mathbf{q}^*} = -\mu = -\partial \bar{E}(N,\mathbf{Q})/\partial N|_{\mathbf{q}=\mathbf{q}^*} \quad (19)$$

where $Q(\mathbf{q}) = \sum_{i=1}^m q_i = \mathbf{q}\mathbf{1}^{\mathrm{T}}$ stands for the overall electric charge of the molecule. In eqs 17−19 we have indicated that this electronegativity equalization takes place only for the equilibrium AIM charges

$$\mathbf{q}^* = (q_1^*, q_2^*, ..., q_m^*) = \mathbf{N}^* - \mathbf{Z} \equiv \mathbf{q}(N,\mathbf{Q}) \quad (20)$$

which are uniquely determined by the system geometry **Q** and the overall number of electrons *N*. The "starting" molecular charges **q** may be obtained, e.g., from the independent SCF MO calculations; we assume that the AIM charges **q** preserve the correct overall charge of a molecular system under consideration.

The electronegativity differences of eq 17 determine the forces triggering the subsequent charge transfer (CT) flows of electrons, $\Delta \mathbf{N}^* = -\Delta \mathbf{q}^*$, corresponding to the transition from the starting AIM charges **q** to the equilibrium values $\mathbf{q}^* = \mathbf{q}(N,\mathbf{Q})$. It follows from the electronegativity equalization equations (eq 18) and the closure relation

$$\Delta N = \sum_{i=1}^m \Delta N_i^* = -\sum_{i=1}^m \Delta q_i^* = -\Delta \mathbf{q}^* \mathbf{1}^{\mathrm{T}} = -\Delta Q = 0 \quad (21)$$

that the unknown CT displacements $\Delta \mathbf{q}^*$ are linked to the forces $\Delta \mathbf{u}^*$ via the following generalized hardness transformation **H**:

$$(\Delta\chi = 0, \Delta \mathbf{q}^*)\begin{pmatrix} 0 & \mathbf{1} \\ \mathbf{1}^{\mathrm{T}} & \mathbf{h} \end{pmatrix} \equiv \Delta \mathbf{X}\,\mathbf{H} = [\Delta Q^* = 0, \Delta \mathbf{u}^*] \equiv \Delta \mathbf{Y} \quad (22)$$

Therefore, the inverse of **H**, $\mathbf{S} = \mathbf{H}^{-1}$, determining the corresponding generalized softness matrix, tranforms $\Delta \mathbf{Y}$ into $\Delta \mathbf{X}$

$$\Delta \mathbf{Y}\,\mathbf{S} = [\Delta Q^* = 0, \Delta \mathbf{u}^*]\begin{pmatrix} \eta & \mathbf{f} \\ \mathbf{f}^{\mathrm{T}} & \mathbf{B} \end{pmatrix} = [\Delta\chi = 0, \Delta \mathbf{q}^*] = \Delta \mathbf{X} \quad (23)$$

where we have identified the following blocks of **S**:

(i) the global hardness η (inverse of the global softness *S*):

$$(\mathbf{S})_{Q,Q} = (\partial\chi/\partial Q)_{\mathbf{u}^*,\mathbf{Q}} = \eta = (\partial\mu/\partial N)_{\mathbf{u}^*,\mathbf{Q}} \equiv S^{-1} \quad (24)$$

(ii) the AIM linear response matrix **B**:

$$(\mathbf{S})_{\mathbf{u},\mathbf{u}} = (\partial \mathbf{q}^*/\partial \mathbf{u}^*)_{Q,\mathbf{Q}} \equiv \mathbf{B}(N,\mathbf{Q}) \quad (25)$$

(iii) the electronic Fukui Function (FF) **f**:

$$(\mathbf{S})_{Q,\mathbf{u}} = (\partial \mathbf{q}^*/\partial Q)_{\mathbf{u}^*,\mathbf{Q}} = (\partial \mathbf{N}^*/\partial N)_{\mathbf{u}^*,\mathbf{Q}} = (\mathbf{S})_{\mathbf{u},Q}{}^{\mathrm{T}} = (\partial\chi/\partial \mathbf{u}^*)_{Q,\mathbf{Q}} \equiv \mathbf{f} \quad (26)$$

Alternatively, as shown elsewhere,[1,3,4] the solution of the electronegativity equalization problem in the closed molecular system can be obtained through the inversion of the so-called internal hardness matrix in the AIM resolution, in which the closure constraint of eq 21 has already been incorporated.

EF Mapping Relations in Closed Systems. It follows from eqs 23 and 25 that in the closed molecular system, for a given molecular geometry **Q**, the displacements of the AIM charges from their equilibrium values are related to the corresponding displacements in the AIM electronegativities through the linear response matrix **B**: $\Delta \mathbf{q}^* = \Delta \mathbf{u}^* \mathbf{B}$.

Clearly, the equilibrium charges $\mathbf{q}_0^* = \mathbf{q}(N,\mathbf{Q}_0)$ for the starting geometry $\mathbf{Q}_0$ are the displaced charges for another (displaced) geometry **Q** of the system under consideration, $\mathbf{q}_0^* \neq \mathbf{q}^* \equiv \mathbf{q}(N,\mathbf{Q})$. Therefore, a general displacement of the atomic electronegativities from the equilibrium (equalized) values can be realized not only through shifting electrons for the fixed *N* and **Q**, but also via changing the system geometry for the fixed initial AIM charges $\mathbf{q}_0^*$.

Thus, we can distinguish the following two contributions to the displacements of the equilibrium (equalized) electronegativities, when geometry is shifted for constant *N* by

$$\Delta \mathbf{Q} = \mathbf{Q} - \mathbf{Q}_0 \quad (27)$$

from the initial geometry $\mathbf{Q}_0$.

The first contribution represents the shift $\Delta \mathbf{u}(N,\Delta \mathbf{Q})$ due to $\Delta \mathbf{Q}$ for the "frozen" starting AIM charges $\mathbf{q}_0^*$, equilibrium for the initial geometry $\mathbf{Q}_0$

$$\mathbf{u}_0^* = \mathbf{u}^*(\mathbf{q}_0^*,\mathbf{Q}_0) = \chi_0 \mathbf{1} \quad (28)$$

These shifts

$$\Delta \mathbf{u}(N,\Delta \mathbf{Q}) = \Delta \mathbf{Q}(\partial \mathbf{u}^*/\partial \mathbf{Q})_{\mathbf{q}_0^*} \equiv \Delta \mathbf{Q}\mathbf{G} \quad (29)$$

differentiate the AIM chemical potentials, thus creating the CT forces $\Delta \mathbf{u}^*(\mathbf{q},\mathbf{Q})$, subsequently restoring the equilibrium electron distribution for the new geometry **Q** after the charge relaxation

$$\Delta \mathbf{q}(\Delta \mathbf{Q}) \equiv -[\mathbf{q}(N,\mathbf{Q}_0) - \mathbf{q}(N,\mathbf{Q})] = -\Delta \mathbf{Q}\mathbf{G}\mathbf{B} \quad (30)$$

Hence, for the closed system the EF−CSA/AIM translator of eq 5 is identified[4,8] as the matrix

$$\mathbf{T}(\mathbf{Q} \rightarrow \mathbf{q})_Q \equiv (\partial \mathbf{q}^*/\partial \mathbf{Q})_Q = -\mathbf{T}(\mathbf{Q} \rightarrow \mathbf{N})_N \equiv -(\partial \mathbf{N}^*/\partial \mathbf{Q})_N \equiv -\mathbf{G}\mathbf{B} \quad (31)$$

It has been shown elsewhere[8] that in the case of the externally open molecular systems (in contact with the hypothetical electron reservoir *R*, which controls the system chemical potential $\mu = -\chi = \mu_R$) the corresponding EF-mapping

translator is obtained by replacing in eq 31 the linear response matrix **B** with the AIM softness matrix

$$\mathbf{s} = (\partial \mathbf{q}/\partial \mathbf{u})_{\chi} = \mathbf{h}^{-1} \tag{32}$$

related to **B** through the Berkowitz−Parr relation[28] in the AIM resolution[1−8] (see also eqs 24 and 26):

$$\mathbf{B} = -\mathbf{s} + \mathbf{f}^{\mathrm{T}} S \mathbf{f} \tag{33}$$

Hence, for the open molecular systems the EF translator in the atomic resolution

$$\mathbf{T}(\mathbf{Q} \rightarrow \mathbf{q})_{\chi} \equiv (\partial \mathbf{q}^*/\partial \mathbf{Q})_{\chi} = -\mathbf{T}(\mathbf{Q} \rightarrow \mathbf{N})_{\mu} \equiv -(\partial \mathbf{N}^*/\partial \mathbf{Q})_{\mu} \equiv -\mathbf{G}\mathbf{s} \tag{34}$$

Geometrical Matrix G. The matrix **G** defined by eq 29 reflects the **Q** dependence of the AIM electronegativities (see eq 16)

$$\mathbf{u}(\mathbf{q}_0^*, \mathbf{Q}) = \mathbf{u}^0 + \mathbf{q}_0^* \mathbf{h}(\mathbf{Q}), \quad \text{or}$$

$$\chi_l = \chi_l^0 + \sum_{i=1}^{m} q_{0,i}^* \eta_{i,l}^0, \quad l = 1, 2, ..., m \tag{35}$$

only through the AIM hardness matrix. It should be noticed that in the CSA parametrization only the off-diagonal hardnesses (eq 12) are geometry dependent, through the internuclear distances $\{R_{ij}\}$. Therefore, the **G** matrix can be evaluated using the chain rule

$$G_{k,l} \equiv (\partial \chi_l/\partial Q_k)_{\mathbf{q}_0^*} = \sum_{i \neq l} q_{0,i}^* (\partial \eta_{il}^0/\partial R_{il})\,(\partial R_{il}/\partial Q_k), \quad k, l = 1, 2, ..., m \tag{36}$$

3. Illustrative Applications

Calculations. We have selected a few small molecules and model molecular complexes to test a performance of the closed-system translator matrix of eq 31, by comparing the charge variation trends it predicts, when some internuclear distances are increased, with the corresponding variations following from both the repeated CSA calculations for different geometries and those resulting from the SCF MO and DFT calculations. The latter have been supplemented by several partitioning schemes of the ground-state electron density into the AIM populations, which define alternative atomic discretizations.

The selected molecular systems include diatomics HX, X = F, Cl, Br, water, ethane, and three molecular adducts, HF- - -HF, H_2O- - -HCl, and ClH- - -NH_3. The SCF MO methods used cover both the representative semiempirical (valence-electron) MNDO (MOPAC6)[18] approximation and the ab initio Hartree−Fock [Gaussian 94/DFT, HF/6-311G(d,p)][17] and Kohn−Sham (DMol, LSDA/DZVP)[19] calculations. The applied AIM division procedures include the Mulliken populational analysis,[20] topological partitioning of Bader,[21] stockholder scheme of Hirshfeld,[22,30] and fitting of the AIM charges to molecular electrostatic potentials.[23] In the MNDO calculations two sets of the Mulliken AIM charges were considered: first, taking into account the nonvanishing overlap of the valence orbitals on different atoms, and second, neglecting these integrals, in full conformity with the ZDO approximation.

When modifying a given geometrical coordinate in a polyatomic system one can monitor variations of the AIM charges for the rigid or relaxed values of the remaining geometrical degrees of freedom. Both these types of charge-variation trends have been examined. In the CSA case the equilibrium geometries obtained from the reference SCF MO calculations have been used.

For a molecular adduct A- - -B both the (intramolecular) polarization (P)- and (intermolecular) global (CT)-stage equilibria[1,3] can be determined from the CSA calculations,[1,3,31] corresponding to the thermodynamical systems (A | B) and (A ⋮ B), respectively, where | represents a hypothetical barrier preventing the intermolecular CT and ⋮ symbolizes a removal of this constraint. In the HF- - -HF case we have reported both the CSA P and CT results, while for the remaining complexes only the P trends are reported. This is because the CSA global electronegativities of different interacting monomers (at the P stage), obtained from the intrasubsystem electronegativity equalization equations, are of not sufficient accuracy to warrant the reliable CT predictions. In the equal sybsystem case, HF- - -HF, these errors cancel to a large degree in the electronegativity difference, which determines the direction and the size of the intersubsystem CT, and the proper asymptotic ($R_{AB} \rightarrow \infty$) behavior of a disscociation into the neutral molecules is assured.

One should recall at this point that the integer number of electrons in the dissociation products can only be obtained in the DFT-type models, when the chemical potential discontinuity[32] is properly accounted for. In the electronegativity equalization description of interactions between an electron acceptor A (acid) and donor B (basis), this requires the biased electronegativities of reactants, $\chi_A = A_A$ and $\chi_B = I_B$, where A_A and I_B denote the electron affinity and ionization potentials of the two interacting but mutually closed subsystems in the $(A \mid B)$ system, respectively.

Molecules. In Figures 1−3 we have summarized the AIM charge variations accompanying the bond stretching in the three HX systems, with panels A and B in each figure corresponding to a comparison of the CSA curves (and the mapping relation tangent lines) with the corresponding SCF MO and DFT plots, respectively. The H_2O results are summarized in Figure 4, while Figure 5 examines variations of the carbon charges in ethane, when the C−C bond is elongated; both these figures compare the MNDO and CSA results.

In Figures 1−3 the EF mapping trends are indeed seen to be tangent at the starting geometry point R_{HX}^0, for which the transformation has been calculated, to the relevant CSA curves obtained from an interpolation of the CSA results for different values of R_{HX}. This validates the algorithm described in the preceding section.

Another general observation following from the HX analysis of Figures 1−3 is that the main trends in responses of the electron distribution to a bond elongation are strongly *method-dependent.* Both the types of the electronic structure theory and the density partitioning scheme are seen to have a strong effect on the predicted AIM charge variations.

The general CSA trend in Figure 1 predicts a monotonic decrease in charge separation $H^{+\delta}-F^{-\delta}$ with increasing R_{HF}, consistent with the atomic diabatic state, which dissociates into atoms: $H^0 + X^0$. This is also in agreement with an elementary "thermodynamical" description, since the greater the bond length, the lower electrostatic influence of the net charge of one atom on the level of the chemical potential/electronegativity of the other atom. For example, an increase in the bond length lowers the chemical potential of $H^{+\delta}$ (electron donor, basic atom perturbed by $F^{-\delta}$) and raises the chemical potential of $F^{-\delta}$ (electron acceptor, acidic atom perturbed by $H^{+\delta}$), thus diminishing the amount of the H → F charge transfer. This is also

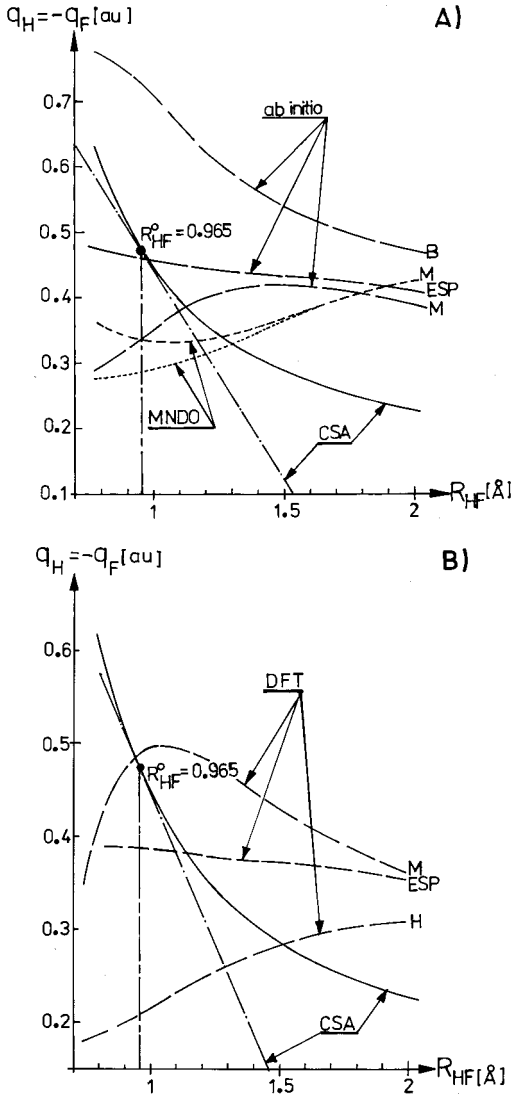

Figure 1. Comparison between the CSA, SCF MO (panel A) and DFT (panel B) trends of variations in atomic charges, accompanying changes in the bond length of HF. The illustrative CSA electron following mapping derivative, shown in both panels as the tangent (dotted-broken) line, has been determined at $R^0_{HF} = 0.965$ Å. The methods used to determine the ground-state electronic structure include the semiempirical (MNDO) and ab initio (Hartree−Fock and Kohn−Sham) theories. The atomic charges shown in the figure include the following partitioning schemes of the molecular electron density: Bader (B), Hirshfeld (H), Mulliken (M), and the charges fitted to reproduce the molecular electrostatic potential (ESP). In the MNDO case the Mulliken charges obtained from the populational analysis taking into account (broken line) and neglecting (dotted line) the overlap between the basis set of the valence-shell atomic orbitals (AO) on different atoms are shown in panel A. A similar convention has been adopted in Figures 2 and 3.

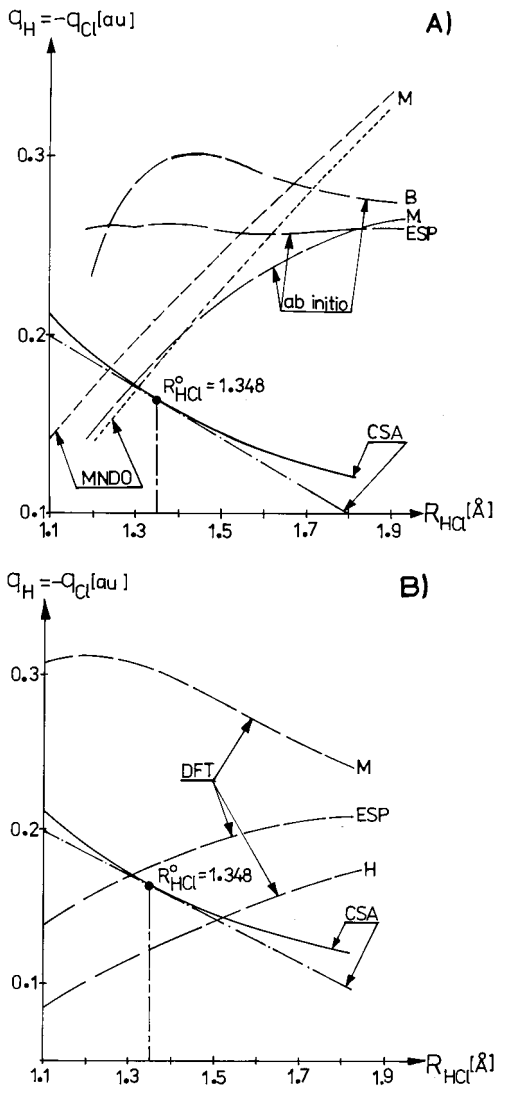

Figure 2. Same as in Figure 1 for HCl.

the physical reason for a qualitatively similar CSA trends observed for HCl (Figure 2) and HBr (Figure 3).

The electronegativity equalization (CSA) charges at larger internuclear separations are seen in Figure 1A (H−F) to exhibit trends generally parallel to those observed in the ab initio B and DFT-M charges. These results are qualitatively opposite to the MNDO M predictions; both overlap variants predict similar trends, with the charge plots diverging more strongly at smaller distances. In both the ab initio SCF MO and DFT cases the Mulliken scheme first exhibits a trend indicating a dissociation into ions and then, at large separations, a dissociation into atoms.

The SCF MO Mulliken charges in Figures 2A and 3A exhibit a qualitatively opposite behavior to the CSA curves of increasing charge separation with bond elongation, which is typical of the ionic diabatic state, leading to the dissociation into ions: $H^+ + X^-$. A similar behavior is detected for the Hirshfeld charges obtained from the DFT calculations (Figures 1B, 2B, 3B) and the DFT ESP charges (Figures 2B, 3B). Notice the qualitatively incorrect behavior of the DFT AIM charges at large separations. Indeed, the KS scheme is known to predict fractional asymptotic charges at the separated atom limit $R_{HX} \rightarrow \infty$.

The ESP charges (fitted to the electrostatic potential) obtained from the ab initio SCF MO (Figures 1A, 2A, 3A) and the DFT calculations (Figure 1B) are relatively resistant to bond stretches, roughly preserving the AIM charge magnitudes. This is not the case in the Kohn−Sham calculations for HCl (Figure 2B) and HBr (Figure 3B), where the ESP plots run in a direction parallel to the H curves.

The charges for the HX systems are also widespread. The CSA is found to consistently predict the lowest charges at large distances. In the range of the equilibrium bond lengths, which roughly correspond to the vicinity of the R^0_{HX} point, the CSA charges are generally in the range of values predicted by other methods.

Let us now examine the four AIM charge panels for water (Figure 4). For the symmetrical stretch of the two bonds (Figure 4A) one observes that the CSA trends (lower panel) are similar to those predicted by the relaxed angle MNDO calculations

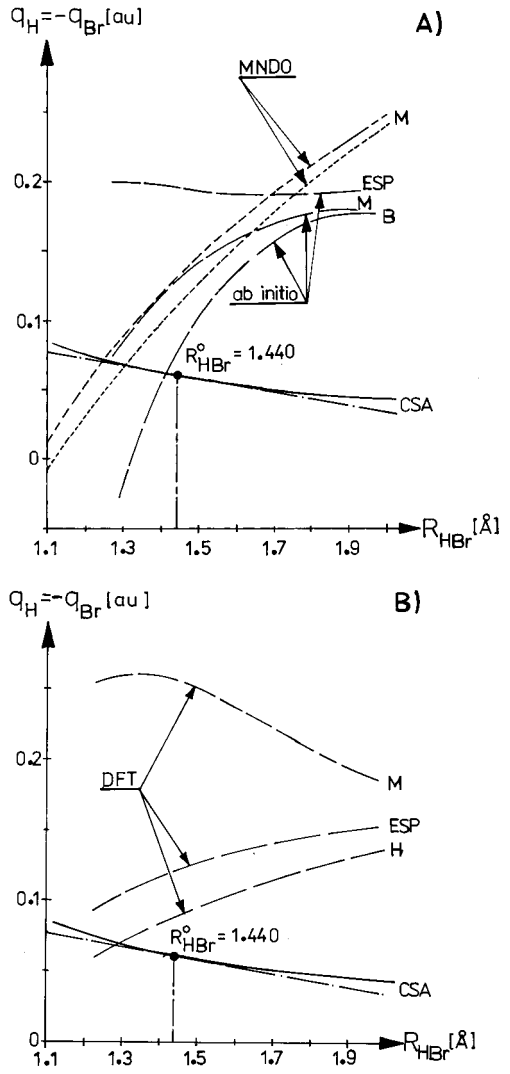

Figure 3. Same as in Figure 1 for HBr.

(upper panel). While the angle relaxation in the MNDO scheme changes the charge variation trend qualitatively, it is seen to have little effect in the CSA case. Again, the CSA trend is consistent with the bond dissociation into atoms; the CSA charges are found to be much smaller than those predicted by the reference MNDO calculations.

These observations generally hold in Figure 4B, where the AIM charge variations for a given stretch of a single ($O-H_1$) bond are examined. In the CSA case one observes a decay in the hydrogen charge of the elongated bond (dissociation to atoms), for a practically unchanged charge of the other, H_2 hydrogen. In the MNDO case the H_2 hydrogen slightly increases its charge when the $O-H_1$ bond is elongated, which manifests a more ionic $O-H_2$ bond. A magnitude of the MNDO charge on oxygen remains roughly unchanged, when a single bond is elongated, while the CSA predicts the O curves approximately parallel to the H_1 ones. As seen in the lower panel of Figure 4B, the CSA mapping transformations provide a semiquantitatively correct CSA trend in a relatively wide range of the bond length displacements.

The bond elongation trends exhibited by the carbon charges in ethane (Figure 5) are seen to be strongly affected by the geometry relaxation in both the MNDO and CSA calculations. In the CSA case (lower panel) the rigid geometry trend (broken line) is practically idinstinquishable from the CSA mapping line calculated for R^0_{CC}.

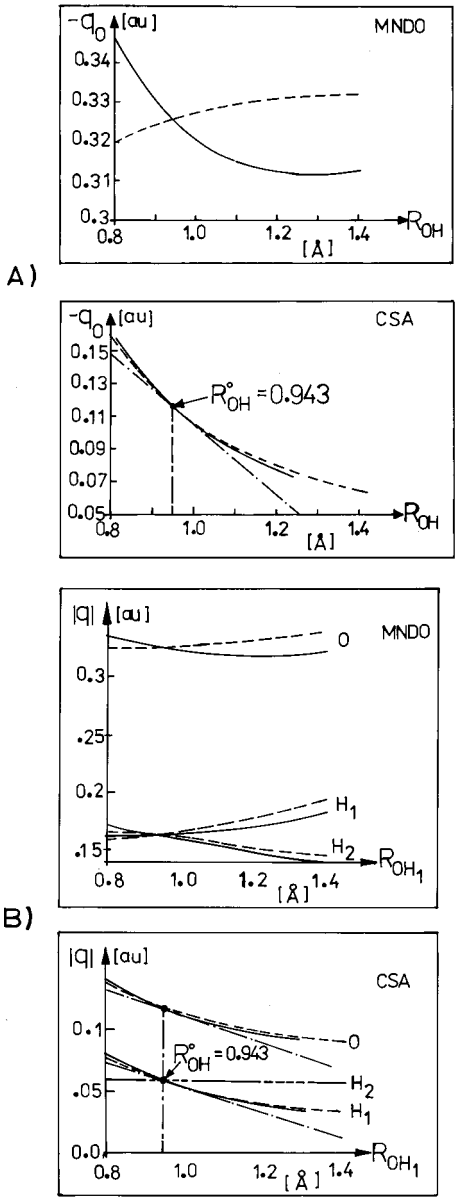

Figure 4. Illustrative plots of changes in the H_2O atomic charges [CSA and MNDO (Mulliken, overlapping AO basis)] with the symmetrical (part A) and nonsymmetrical (part B) stretches of the O−H bond(s) for the rigid (MNDO equilibrium bond angle, broken line) and relaxed (solid line) geometries. In part B, the H_1 denotes the hydrogen of the elongated bond. Throughout the figure, boken and solid lines correspond to the rigid and MNDO relaxed molecular geometries, respectively. The CSA mapping derivatives, represented by the corresponding tangent lines (dotted-boken), have been generated for the equilibrium MNDO geometry ($R^0_{OH} = 0.943$ Å). A similar convention is adopted in Figure 5.

Molecular Adducts. The AIM charge variations accompanying changes of the intermolecular separation R_{AB} in the representative molecular complexes A- - -B are the subject of the remaining three Figures 6−8. In the HF- - -HF case (Figure 6) the CT stage CSA results for both monomers (part B) are compared with the corresponding predictions obtained from the ab initio and MNDO calculations (part A); the latter correspond to the global ground-state equilibrium in the complex as a whole. The diagrams for the H_2O- - -HCl (Figure 7) and ClH- - -NH_3 (Figure 8) complexes similarly compare the MNDO supermolecule AIM charges with those resulting from the P-stage (intramonomer polarization) CSA predictions.

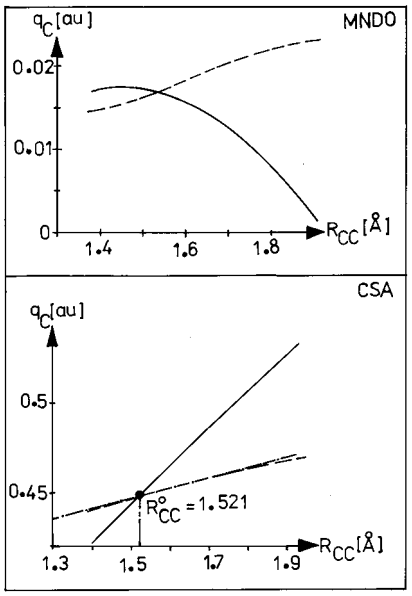

Figure 5. Same as in Figure 4 for stretching the C−C bond in ethane. In the lower panel the CSA rigid geometry and the mapping (for R^0_{CC} = 1.521 Å) lines are practically identical.

Since the coordinating atoms $-F^{\delta-}\cdots H^{\delta+}-$ of both subsystems in the linear adduct (H−F | H−F) (at the polarization, P-stage) exert the dominating influence on the level of the chemical potential/electronegativity of the other subsystem, one predicts an increase in the chemical potential (decrease of electronegativity) of the right molecule (perturbed by $F^{\delta-}$) and a decrease in the chemical potential (increase of electronegativity) of the left molecule (perturbed by $H^{\delta+}$), when both molecules apprach one another from the initial infinite separation. Therefore, in the CSA approach the right molecule must act as the electron donor (a base B) and the left molecule as the electron acceptor (an acid A) in the CT system (H−F ⋮ H−F), when the barrier preventing the $A \leftarrow B$ CT is lifted. This is indeed reflected by the AIM charge variations in Figure 6B, where we have also identified the trends associated with the secondary, CT-induced polarizations inside monomers.

A reference to Figure 6A indicates that the opposite directions of these CT and CT-induced P flows of electrons are predicted in both the ab initio and MNDO supermolecule calculations.

It should be realized that in such an energetically preferred complementary arrangement of both monomers the above dominating perturbations due to the coordinating atoms also induce the initial polarizations of monomers in the direction

$$H \xrightarrow{P} F \;\big|\; H \xrightarrow{P} F$$

which increase the initial charge accumulation (depletion) on the F(H) atom of the separated monomers.[33] This prediction is in agreement with the first Gutmann rule.[14] This polarization stage is reflected by the broken lines in Figure 6B. They indeed exhibit stronger bond polarizations inside each mutually closed, but interacting monomer, relative to the separated monomer levels. Notice also that both the hydrogen atom of the acceptor molecule and the fluorine atom of the donor molecule lower the magnitudes of their charges, as a result of the CT-indiced polarizations, which act in the reverse direction to the primary polarizations at the P stage, in the spirit of the familiar Le Châtelier−Braun principle of thermodynamics.[34]

It also follows from Figure 6B that the short-range mapping trends are valid only in the region of strong (chemical) inter-

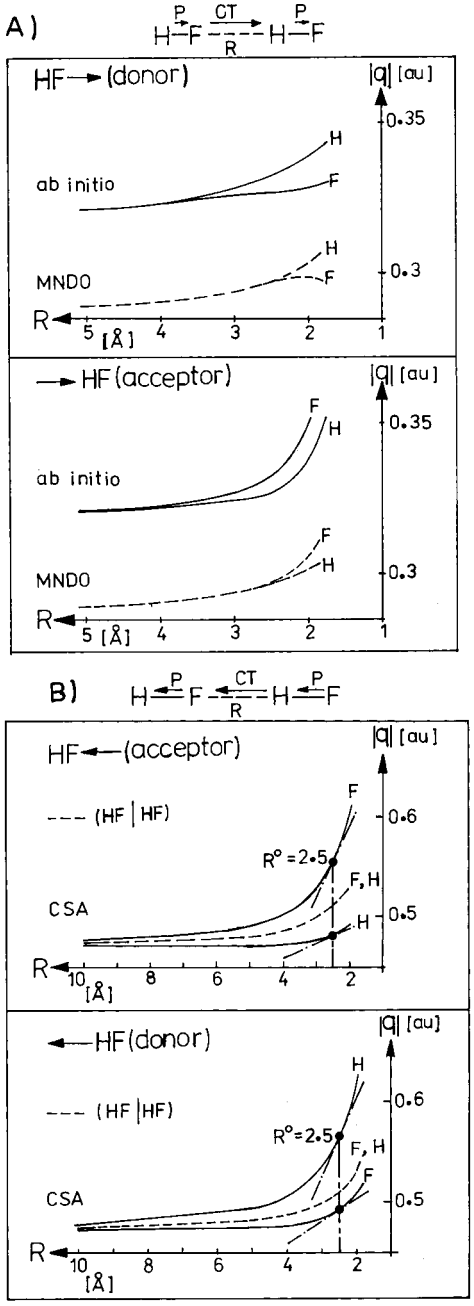

Figure 6. Comparison of the charge reorganization patterns in the HF−HF complex, predicted within the SCF MO (ab initio and MNDO, part A) and CSA (part B) approximations. Representative CSA mapping derivatives for the intermolecular separation R^0 = 2.5 Å are also shown as the lines (dotted-broken) tangent to the corresponding CSA charge variation curves. The broken lines in the CSA panels correspond to the mutually and externally closed, but interacting, molecules which can only polarize their electron density for the fixed subsystem number of electrons. This is symbolized by the (HF|HF) notation, in which the vertical solid line stands for a hypothetical "wall" preventing the intermolecular CT. The global equilibrium in the molecular complex (CT stage of the interaction between the two molecules) is accordingly denoted by (HF⋮HF), with the broken vertical line to emphasize that this barrier has been removed. The indicated flows of electrons represent displacements in the atomic electron populations due to the intermolecular charge transfer (CT) and the CT-induced, intramolecular polarization (P). It follows from the figure that the polarization-only CSA trends, exhibited by the (HF|HF) curves, are in qualitative agreement with the SCF MO predictions. However, the CSA (part A) predicts the opposite CT direction, and thus also the opposite trends of the accompanying P adjustments, to those predicted by the SCF MO methods (part A). A similar convention has been adopted in Figures 7 and 8.

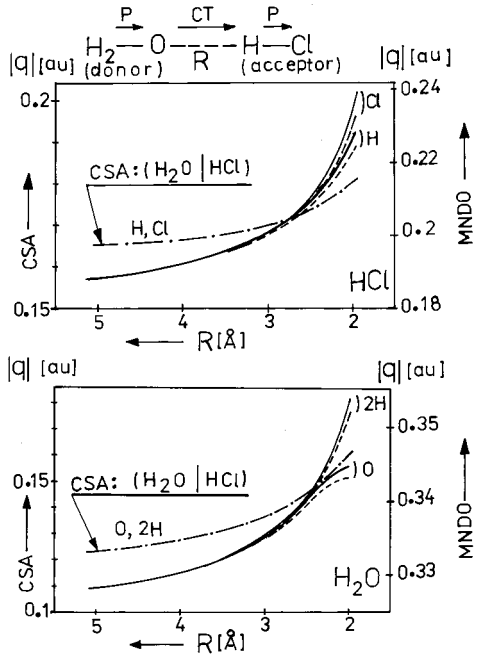

Figure 7. Same as in Figure 6 for the H_2O- - -HCl complex. The solid and broken lines correspond to the MNDO-relaxed and rigid molecular geometries, respectively. The CSA predictions are limited to the intramolecular polarization trend only.

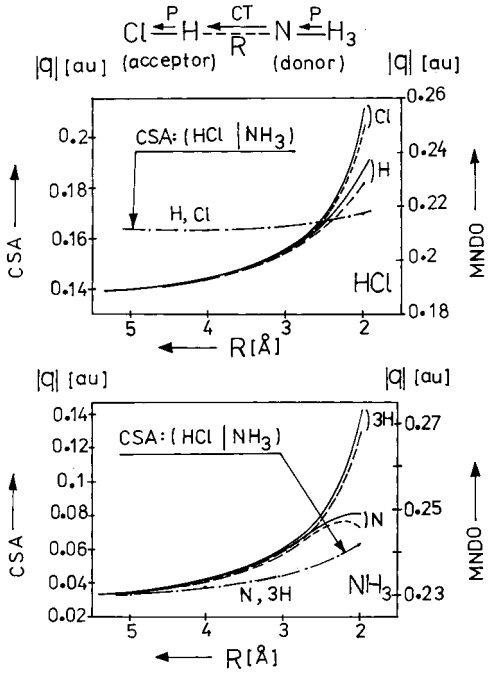

Figure 8. Same as in Figure 7 for the ClH- - -NH_3 complex.

actions, since the tangent direction quickly changes with increasing separation between monomers.

Turning now to the H_2O- - -HCl plots of Figure 7, one concludes from the SCF MO charge variation plots that water molecule acts as an electron donor (basic) reactant while HCl represents an electron acceptor (acidic) reactant. The $H_2O \rightarrow$ HCl charge transfer in (H_2O : HCl) also rationalizes the CT-induced flows inside both molecules, which are also shown in the figure. The P-stage variations of the CSA charges predict increased bond polarizations inside both mutually closed molecules in (H_2O | HCl).This intermediate charge rearrangement increases the donor ability of the coordinating oxygen atom of the water molecule and the acceptor capacity of the hydrogen atom of HCl, thus increasing the amount of the subsequent $H_2O \rightarrow$ HCl CT, when the barrier for the intermonomer CT is lifted. Notice again that the CT-induced intramonomer polarization flows moderate the increase in the magnitude of charges of the coordinating atoms due to the primary $(H_2)O \rightarrow H(Cl)$ flow of electrons, in accordance with the Le Châtelier−Braun principle of thermodynamics.

Similar conclusions follow from Figure 8 for the ClH- - -NH_3 complex, where the left molecule acts as an acid and the right molecule is a base. Again, the CSA P-trends exhibit relatively small increase in charge magnitude when the separation between the two molecules decreases. Thus, the CT charge displacements again dominante the overall charge reconstruction patterns on both molecules.

4. Conclusion

We have demonstrated in this work, how the electronegativity equalization principle of Sanderson can be used within the CSA to derive the explicit electron-following mapping transformations for the closed molecular systems. The relevant "translator" matrix $\mathbf{T}(\mathbf{Q} \rightarrow \mathbf{q})_Q$ is found to be given by the negative product of a straightforward geometrical matrix **G**, the elements of which reflect a geometry dependence of the CSA atomic charges through the off-diagonal elements of the AIM hardness matrix, and the familiar linear response matrix **B** in the atomic resolution.

These direct electron-following charge-reconstruction trends have been numerically validated by comparing them with the plots of the AIM charges obtained from several CSA calculations, for changing molecular geometry. Indeed, the "translator" lines $\Delta\mathbf{q}_T(\mathbf{Q};\mathbf{Q}_0)$, determined for a a given initial geometry $\mathbf{Q}_0$, were shown to be tangent at $\mathbf{Q}_0$ to the corresponding exact CSA curves, $\Delta\mathbf{q}_{CSA}(\mathbf{Q})$.

The mapping transformations were shown to provide semiquantitative indicators of the CSA charge reorganization accompanying conformational changes in a single molecule, and during a mutual approach of reactants forming a molecular complex. Therefore, they represent an important extension of the charge sensitivity analysis, by providing means to directly diagnose the atomic charge variations in response to displacenments (real or hypothetical) in molecular geometry without any supplementary CSA calculations.

The extensive comparison carried out for the hydrogen halide systems indicates that no unique EF interpretation of the bond stretch reconstruction of atomic charges emerges from several electronic structure calculations and alternative AIM partitioning schemes. Such interpretations are thus found to be strongly method dependent.

Acknowledgment. This work was supported by a research grant from the State Committee for Scientific Research in Poland. We thank Prof. J. Mrozek and Dr. J. Korchowiec for their help in generating the numerical results.

References and Notes

(1) Nalewajski, R. F.; Korchowiec, J. *Charge Sensitivity Approach to Electronic Structure and Chemical Reactivity*; World-Scientific: Singapore, 1997.

(2) Baekelandt, B.; Mortier, W. J.; Schoonheydt, R. A. In *Structure and Bonding, Vol. 80: Chemical Hardness*; Sen, K. D., Ed.; Springer-Verlag: Berlin, 1993; p 187. Janssens, G. O. A.; Mortier, W. J.; Schoonheydt, R. A. In *Developments in the Theory of Chemical Reactivity and Heterogeneous Catalysis*; Mortier, W. J., Schoonheydt, R. A., Eds.; Research Signpost: Trivandrum, India, 1997; p 45.

(3) Nalewajski R. F.; Korchowiec, J.; Michalak, A. In *Topics in Current Chemistry, Vol. 183: Density Functional Theory IV−Theory of Chemical Reactivity*; Nalewajski, R. F., Ed.; Springer-Verlag: Heidelberg, Germany, 1996; p 25.

(4) Baekelandt, B. G.; Janssens, G. O. A.; Toufar, H.; Mortier, W. J.; Schoonheydt, R. A.; Nalewajski, R. F. *J. Phys. Chem.* **1995**, *99*, 9784.

(5) Nalewajski, R. F. In *Proceedings of a NATO ASI on Density Functional Theory, Il Ciocco, August 16−27, 1997*; Dreizler, R. M., Gross, E. K. U., Eds.; Plenum: New York, 1995; p 339.

(6) Janssens, G. O. A.; Baekelandt, B. G.; Toufar, H.; Mortier, W. J.; Schoonheydt, R. A. *Int. J. Quantum. Chem.* **1995**, *56*, 317. Janssens, G. O. A.; Mortier, W. J.; Schoonheydt, R. A. In *Developments in the Theory of Chemical Reactivity and Heterogeneous Catalysis*; Mortier, W. J., Schoonheydt, R. A., Eds.; Research Signpost: Trivandrum, India, 1997; p 135.

(7) Nalewajski, R. F. *Phys. Chem. Chem. Phys.* **1999**, *1*, 1037.

(8) Nalewajski, R. F. *Comput. Chem.*, in press.

(9) Kohn, W.; Sham, L. J. *Phys. Rev.* **1965**, *140A*, 1133.

(10) Hohenberg, P.; Kohn, W. *Phys. Rev.* **1964**, *136B*, 864.

(11) Parr, R. G.; Yang, W. *Density Functional Theory of Atoms and Molecules*; Oxford: New York, 1989.

(12) Nalewajski, R. F., Ed. *Topics in Current Chemistry: Density Functional Theory*; Springer-Verlag: Heidelberg, Germany, 1996; Vols. 180−183.

(13) Anderson, A. B.; Parr, R. G. *J. Chem. Phys.* **1970**, *53*, 3375; **1971**, *55*, 5490.

(14) Gutmann, V. *The Donor−Acceptor Approach to Molecular Interactions*; Plenum: New York, 1978.

(15) Nakatsuji, H. *J. Am. Chem. Soc.* **1974**, *96*, 24, 30.

(16) Jones, L. H.; Ryan, R. R. *J. Chem. Phys.* **1970**, *52*, 2003. Decius, J. C. *J. Chem. Phys*. **1976**, *98*, 3067.

(17) Frish, M. J.; Trucs, G. W.; Schlegel, H. B.; Gill, P. M. W.; Johnson, B. G.; Robb, M. A.; Cheeseman, J. R.; Keith, T.; Petersson, A. A.; Montgomery, J. A.; Raghavachari, K.; Al-Laham, M. A.; Zakrzewski, V. G.; Ortiz, J. V.; Foresman, J. B.; Ciosłowski, J.; Stefanov, B. B.; Nanayakkara, A.; Challacombe, M.; Peng, C. Y.; Ayala, P. Y.; Chen, W.; Wong, M. W.; Andres, J. L.; Replogle, E. S.; Gomperts, R.; Martin, R. L.; Fox, D. J.; Binkley, J. S.; Defrees, D. J.; Baker, J.; Stewart, J. P.; Head-Gordon, M.; Gonzales, C.; Pople, J. A. *Gaussian 94/DFT*, Revision D.1; Gaussian, Inc.: Pittsburgh, PA, 1995.

(18) Dewar, M. J. S.; Thiel, W. *J. Am. Chem. Soc.* **1977**, *99*, 4899. Dewar, M. J. S.; Zoebisch, E. G.; Healy, E. F.; Stewart, J. J. P. *J. Am. Chem. Soc.* **1985**, *107*, 3902.

(19) *DMol User Guide, September 1996*; Molecular Simulations: San Diego, CA, 1996.

(20) Mulliken, R. S. *J. Chem. Phys.* **1935**, *3*, 573; **1955**, *23*, 1833.

(21) Bader, R. F. W. *Atoms in Molecules*; Oxford: New York, 1994. Bader, R. F. W.; Nguyen-Dang, T. T. *Adv. Quantum Chem.* **1981**, *14*, 1981. Bader, R. F. W.; Becker, P. *Chem. Phys. Lett.* **1998**, *148*, 452.

(22) Hirshfeld, F. L. *Theor. Chim. Acta* **1977**, *44*, 129.

(23) The atomic charges fitted to reproduce the most the molecular electrostatic potential; ESP options are available in the Gaussian 94/DFT and DMol systems of refs 17 and 19.

(24) Mulliken, R. S. *J. Chem. Phys.* **1934**, *2*, 782.

(25) Pariser, R. *J. Chem. Phys.* **1953**, *21*, 568.

(26) Ohno, K. *Adv. Quantum Chem.* **1967**, *3*, 239; *Theor. Chim. Acta* **1968**, *10*, 111.

(27) Parr, R. G.; Pearson, R. G. *J. Am. Chem. Soc.* **1983**, *105*, 7512.

(28) Berkowitz, M.; Parr, R. G. *J. Chem. Phys.* **1988**, *88*, 2554.

(29) Parr, R. G.; Yang, W. *J. Am. Chem. Soc.* **1984**, *106*, 4049.

(30) Nalewajski, R. F.; Parr, R. G. *J. Am. Chem. Soc.*, in press.

(31) Nalewajski, R. F.; Korchowiec, J. *J. Mol. Catal.* **1996**, *112*, 167. Nalewajski, R. F.; Michalak, A. *J. Phys. Chem.* **1996**, *100*, 20076; *J. Phys. Chem. A* **1998**, *102*, 636.

(32) Gyftopoulos, E. P.; Hatsopoulos, G. N. *Proc. Natl. Acad. Sci. U.S.A.* **1968**, *60*, 786. Perdew, J. P.; Parr, R. G.; Levy, M.; Balduz, J. L. *Phys. Rev. Lett.* **1982**, *49*, 1691.

(33) Chandra, A. K.; Michalak, A.; Nguyen, M. T.; Nalewajski, R. F. *J. Phys. Chem. A* **1998**, *102*, 100182. Nalewajski, R. F. *Top. Catal.*, in press; *Int. J. Quantum Chem.*, in press.

(34) Callen, H. B. *Thermodynamics: An Introduction to the Physical Theories of Equilibrium Thermostatics and Irreversible Thermodynamics*; Wiley: New York, 1960.